
Article:
Docherty, P.J., Girou, C., Derry, M.J. et al. (1 more author) (2020) Epoxy-functional diblock copolymer spheres, worms and vesicles via polymerization-induced self-assembly in mineral oil. Polymer Chemistry, 11 (19). pp. 3332-3339. ISSN 1759-9954

https://doi.org/10.1039/d0py00380h

ARTICLE

Epoxy-Functional Diblock Copolymer Spheres, Worms and Vesicles via Polymerization-Induced Self-Assembly in Mineral Oil

Received 00th January 20xx,
Accepted 00th January 20xx

DOI: 10.1039/x0xx00000x

Philip J. Docherty, Chloé Girou, Matthew J. Derry,†,* and Steven P. Armes*

Epoxy-functional diblock copolymer spheres, worms and vesicles are synthesized via reversible addition-fragmentation chain transfer (RAFT) dispersion polymerization of glycidyl methacrylate (GlyMA) in mineral oil at 70 °C and at 30% w/w solids. This is achieved by using a relatively short oil-soluble poly(stearyl methacrylate) (PSMA) macromolecular chain transfer agent (macro-CTA) with a mean degree of polymerization of 9. Gel permeation chromatography (GPC) studies indicate that good control over the molecular weight distribution can be obtained and the resulting $PSMA_9$-$PGlyMA_x$ nano-objects are characterized by dynamic light scattering (DLS), transmission electron microscopy (TEM) and small-angle X-ray scattering (SAXS). Oscillatory rheology studies of a 30% w/w $PSMA_9$-$PGlyMA_{75}$ worm gel indicate that thermally-triggered degelation occurs on heating to 100 °C. TEM studies indicate that a partial worm-to-vesicle transition occurs under such conditions.

Introduction

Over the past decade there has been considerable interest in using polymerization-induced self-assembly (PISA) to prepare well-defined block copolymer nanoparticles directly in the form of concentrated dispersions.[1-7] During PISA, a soluble polymer is chain-extended in a suitable solvent using a monomer that polymerizes to form an insoluble polymer, thus producing amphiphilic block copolymer chains that self-assemble to form sterically-stabilized nanoparticles during their synthesis. The polymerization technique most commonly utilized for PISA syntheses is reversible addition-fragmentation chain transfer (RAFT) polymerization:[8-10] there are numerous literature examples of RAFT-mediated PISA formulations for polar solvents such as water[11-17] or ethanol.[18-23] Recently, RAFT dispersion polymerization formulations have also been devised for non-polar solvents such as *n*-heptane,[24, 25] *n*-octane,[26, 27] *n*-dodecane,[28] *iso*-dodecane,[29, 30] *n*-tetradecane,[27, 31, 32] mineral oil,[33-37] poly(α-olefins)[33] and silicone oils.[38, 39] The three most common copolymer morphologies obtained via PISA are spheres, worms and vesicles. The final diblock copolymer morphology is primarily dictated by the relative volume fractions of the two blocks, although other parameters such as the mean degree of polymerization (DP) of the soluble steric stabilizer block and the overall copolymer concentration can also be important. Recently, we reported that spherical nanoparticles prepared via PISA directly in mineral oil are potentially useful lubricating additives for the development of next-generation ultralow-viscosity automotive engine oils.[36] In principle, worm-like particles may also be useful as viscosity modifiers for engine oils,[28] while diblock copolymer vesicles may provide a new mechanism for high temperature oil thickening via a thermally-induced vesicle-to-worm transition.[35] Finally, spheres and worms prepared in *n*-dodecane have been examined as Pickering emulsifiers for the stabilization of water-in-oil emulsions.[40, 41]

PISA provides a convenient method of preparing *functional* nanoparticles that can be readily derivatized simply by utilizing reactive monomers such as glycidyl methacrylate,[37, 42-47] pentafluorophenyl methacrylate[27, 48] or 2-(dimethylamino)ethyl methacrylate.[39] Of particular relevance to the present work is the preparation of poly(stearyl methacrylate)-poly(glycidyl methacrylate) [PSMA-PGlyMA] diblock copolymer spheres via RAFT dispersion polymerization in mineral oil, as recently reported by Docherty *et al.*[37] As expected, these nanoparticles exhibit superior long-term stability with respect to hydrolytic degradation (i.e. ring-opening of the epoxy groups by reaction with traces of water) compared to an equivalent aqueous PISA formulation.[44] Moreover, the former epoxy-functional spheres can be readily functionalized with aromatic amines. However, only kinetically-trapped spherical nanoparticles were obtained when using $PSMA_{13}$ or $PSMA_{18}$ as the steric stabilizer block. For many PISA formulations, access to worms or vesicles is facilitated by using a relatively short stabilizer block while also conducting such syntheses at relatively high solids.[24, 25, 28, 33, 34]

In the present study, we utilize a relatively short poly(stearyl methacrylate) PSMA stabilizer block for the preparation of epoxy-functional PSMA-PGlyMA diblock copolymer nanoparticles via RAFT dispersion polymerization in mineral oil. This enables the convenient formation of well-defined epoxy-functional spheres, worms or vesicles, provided that such PISA syntheses are conducted at 30% w/w solids. We believe that

Department of Chemistry, The University of Sheffield, Dainton Building, Brook Hill, Sheffield, South Yorkshire, S3 7HF, UK.
†*Present address: Aston institute of Materials Research, Aston University, Aston Triangle, Birmingham, B4 7ET, UK.*

Electronic Supplementary Information (ESI) available: ^{1}H NMR spectra, summary of SAXS fitting parameters, additional oscillatory rheology data, additional transmission electron microscopy study, SAXS models. See DOI: 10.1039/x0xx00000x

this is the first time that epoxy-functional worms or vesicles have been prepared via PISA in non-polar media. The resulting series of PSMA-PGlyMA nano-objects are characterized using dynamic light scattering (DLS), transmission electron microscopy (TEM) and small-angle X-ray scattering (SAXS). Oscillatory rheology experiments conducted on a 30% w/w $PSMA_9$-$PGlyMA_{75}$ worm gel indicate that degelation occurs on heating to 100 °C, which is attributed to a (partial) worm-to-vesicle morphological transformation.

Experimental

Materials

Glycidyl methacrylate (GlyMA), $CDCl_3$, 2-cyano-2-propyl benzodithioate (CPDB) and all other reagents were purchased from Sigma-Aldrich (UK) and were used as received, unless otherwise noted. Stearyl methacrylate (SMA) was purchased from Santa Cruz Biotechnology Ltd. (USA). tert-Butyl peroxy-2-ethylhexanoate (T21s) initiator was purchased from AkzoNobel (The Netherlands). Toluene, $CHCl_3$ and *n*-dodecane were purchased from Fisher Scientific (UK) and CD_2Cl_2 was purchased from Goss Scientific (UK). API Group III mineral oil (viscosity = 3.1 cSt at 100 °C) was kindly provided by The Lubrizol Corporation Ltd (Hazelwood, Derbyshire, UK).

Synthesis of poly(stearyl methacrylate) (PSMA) macromolecular chain transfer agent (macro-CTA) via RAFT solution polymerization

The synthesis of the $PSMA_9$ macro-CTA via RAFT solution polymerization was conducted as follows: A 250 mL round-bottomed flask was charged with stearyl methacrylate (SMA; 34.0 g; 100 mmol), 2-cyano-2-propyl benzodithioate (CPDB; 4.40 g; 20.0 mmol; target degree of polymerization, DP = 5), 2,2'-azobisisobutyronitrile (AIBN; 659 mg; 4.01 mmol, [CPDB]/[AIBN] molar ratio = 5.0) and toluene (39.0 g). The sealed reaction vessel was purged with nitrogen for 30 min, placed in a pre-heated oil bath at 70 °C and stirred for 4 h. The resulting PSMA homopolymer (SMA conversion = 77%; M_n = 4 200 g mol^{-1}; M_w/M_n = 1.14) was purified by precipitating from toluene into a ten-fold excess of ethanol (twice). The mean degree of polymerization (DP) of this precursor was calculated to be 9 (corresponding to a CPDB efficiency of 43%) using ^{1}H NMR spectroscopy by comparing the integrated signals corresponding to the five aromatic protons at 7.3-7.9 ppm with that assigned to the two oxymethylene protons of PSMA at 3.8-4.2 ppm.

Synthesis of poly(stearyl methacrylate)-poly(glycidyl methacrylate) (PSMA-PGlyMA) diblock copolymer nanoparticles via RAFT dispersion polymerization of glycidyl methacrylate in mineral oil

A typical RAFT dispersion polymerization synthesis of $PSMA_9$-$PGlyMA_{100}$ diblock copolymer nanoparticles at 30% w/w solids was conducted as follows: GlyMA (0.652 g; 4.59 mmol), T21s initiator (1.98 mg; 9.18 μmol; 10% v/v in mineral oil) and $PSMA_9$ macro-CTA (0.15 g; 45.9 μmol; [macro-CTA]/[initiator] molar ratio = 5.0; target PGlyMA DP = 100) were dissolved in mineral oil (1.87 g). The reaction mixture was sealed and purged with nitrogen for 30 min, then the deoxygenated solution was placed in a pre-heated oil bath at 70 °C and stirred for 3 h (final GlyMA conversion = 96% as determined by ^{1}H NMR spectroscopy; M_n = 12 700; M_w/M_n = 1.22).

Gel permeation chromatography (GPC)

Molecular weight distributions were assessed by GPC using chloroform eluent. The GPC set-up comprised two 5 μm (30 cm) Mixed C columns, a HPLC pump and a WellChrom K-2301 refractive index detector operating at 950 ± 30 nm. The mobile phase contained 0.25% v/v triethylamine and the flow rate was fixed at 1.0 mL min^{-1}. A series of twelve near-monodisperse poly(methyl methacrylate) standards (M_p values ranging from 800 to 2 200 000 g mol^{-1}) were used for column calibration.

^{1}H NMR spectroscopy

^{1}H NMR spectra were recorded in either CD_2Cl_2 (to determine the mean DP for the PSMA precursor) or $CDCl_3$ (for all other spectra) using a Bruker AV1-400 MHz spectrometer. Typically, 64 scans were averaged per spectrum. Chemical shifts are expressed in ppm and are internally referenced to the residual solvent peak.

Dynamic light scattering (DLS)

DLS studies were performed using a Zetasizer Nano ZS instrument (Malvern Instruments, UK) at a fixed scattering angle of 173°. Copolymer dispersions were diluted to 0.10% w/w using *n*-dodecane prior to analysis at 25 °C. The intensity-average diameter and polydispersity of the diblock copolymer nanoparticles were calculated by cumulants analysis of the experimental correlation function using Dispersion Technology Software version 6.20. Data were averaged over thirteen runs with each run being of thirty seconds duration.

Transmission electron microscopy (TEM)

TEM studies were conducted using a Philips CM 100 instrument operating at 100 kV and equipped with a Gatan 1 k CCD camera. Copolymer dispersions were diluted to 0.10% w/w using *n*-dodecane, placed on carbon-coated copper grids via pipette and exposed to ruthenium(VIII) oxide vapor for 7 min at 20 °C prior to analysis. This heavy metal compound acted as a positive stain for the core-forming PGlyMA block to improve contrast. The ruthenium(VIII) oxide was prepared as reported previously.[49]

Small-angle X-ray scattering (SAXS)

SAXS patterns were recorded for 1.0% w/w dispersions using a Xeuss 2.0 SAXS instrument (Xenocs, France) equipped with a liquid gallium MetalJet X-ray source (Excillum, Sweden, λ = 0.134 nm), two sets of motorized scatterless slits for beam collimation and a Dectris Pilatus 1M pixel detector (sample-to-detector distance = 5.102 m). SAXS patterns were recorded from q = 0.02 nm^{-1} to q = 1.3 nm^{-1}, where $q = (4\pi \sin\theta)/\lambda$ is the

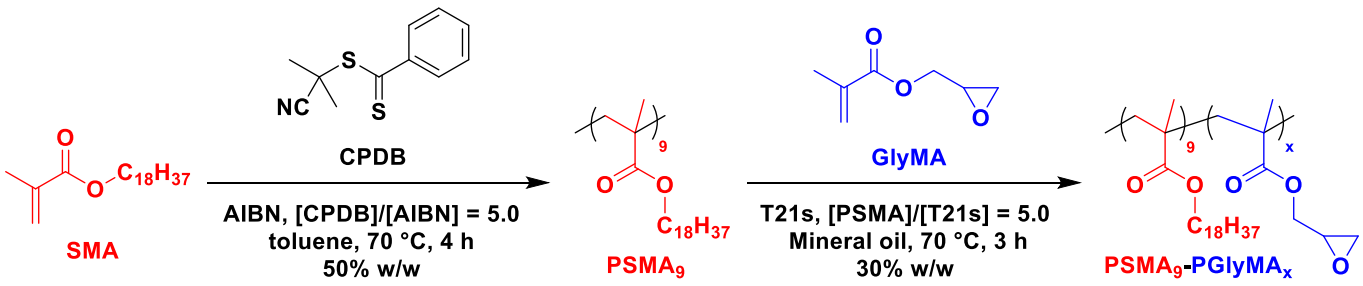

Scheme 1. Synthesis of a poly(stearyl methacrylate) ($PSMA_9$) precursor *via* RAFT solution polymerization of stearyl methacrylate (SMA) in toluene at 50% w/w solids using 2-cyano-2-propyl benzodithioate (CPDB) at 70 °C, followed by the RAFT dispersion polymerization of glycidyl methacrylate (GlyMA) in mineral oil at 70 °C and 30% w/w solids.

length of the scattering vector and θ is one-half of the scattering angle. Glass capillaries of 2.0 mm diameter were used as a sample holder and patterns were recorded and averaged over three 10 min periods. Data were reduced (normalization, integration and averaging) using the Foxtrot software package supplied with the Xeuss 2.0 instrument and further analyzed (background subtraction and data modelling) using Irena SAS macros[50] for Igor Pro.

Oscillatory rheology

An AR-G2 rheometer equipped with a variable temperature Peltier plate and a 40 m*m* 2° aluminium cone was used for all experiments. The percentage strain sweep was conducted at 25 °C using a fixed angular frequency of 10 rad s^{-1}. The angular frequency sweep was conducted at 25 °C using a constant percentage strain of 1.0%. The temperature sweep was conducted on heating from 25 °C to 100 °C at 2 °C min^{-1} at 1.0% strain and an angular frequency of 10 rad s^{-1}, with data being collected every 30 s (which corresponds to each 1 °C interval).

Results and Discussion

A relatively short PSMA homopolymer (mean degree of polymerization = 9) was synthesized at 50% w/w solids via RAFT solution polymerization of SMA using 2-cyano-2-propyl benzodithioate (CPDB) in toluene at 70 °C (see Scheme 1). This polymerization was quenched at 77% conversion in order to avoid monomer-starved conditions, thus preserving the RAFT CTA chain-ends and ensuring the subsequent synthesis of well-defined diblock copolymers. Importantly, this $PSMA_9$ precursor is significantly shorter than the $PSMA_{13}$ and $PSMA_{18}$ stabilizer blocks previously utilized for the formation of kinetically-trapped PSMA-PGlyMA spheres in mineral oil.[37] This $PSMA_9$ block was chain-extended via RAFT dispersion polymerization of GlyMA in mineral oil at 30% w/w solids (see Table 1), with monomer conversions of at least 96% and more than 95% epoxide retention being achieved within 3 h at 70°C, as judged by ^{1}H NMR spectroscopy (see example spectrum shown in Figure 1). The resulting $PSMA_9$-$PGlyMA_x$ diblock copolymers (hereafter denoted S_9-Gly_x for brevity) exhibited a linear increase in M_n with increasing PGlyMA DP (x) and relatively narrow molecular weight distributions (M_w/M_n < 1.30) as judged by gel permeation chromatography (see Figure 2). Efficient chain extension was confirmed by the unimodal nature of the molecular weight distribution curves observed for the $PSMA_9$-$PGlyMA_x$ diblock copolymers, which were shifted to

Table 1. Summary of (co)polymer compositions, monomer conversions, GPC molecular weight data, dynamic light scattering data and transmission electron microscopy nanoparticle morphology assignment (S = spheres, W = worms and V = vesicles) for various $PSMA_9$-$PGlyMA_x$ (denoted S_9-G_x) diblock copolymer nano-objects synthesized via RAFT dispersion polymerization in mineral oil at 70 °C and 30% w/w solids. Molecular weight data obtained for the $PSMA_9$ (S_9) precursor are shown as a reference.

	GlyMA conv. (%)	THF GPC		DLS		TEM
		M_n (kg mol^{-1})	M_w/M_n	D (nm)	PDI	
S_9	-	2.9	1.20	-	-	-
S_9-Gly_{25}	99%	5.8	1.23	27	0.43	S
S_9-Gly_{50}	99%	8.3	1.16	31	0.21	S
S_9-Gly_{75}	99%	10.7	1.20	117	0.24	W
S_9-Gly_{100}	96%	12.7	1.22	325	0.63	W+V
S_9-Gly_{150}	99%	16.6	1.28	170	0.06	V
S_9-Gly_{200}	98%	20.8	1.29	190	0.10	V

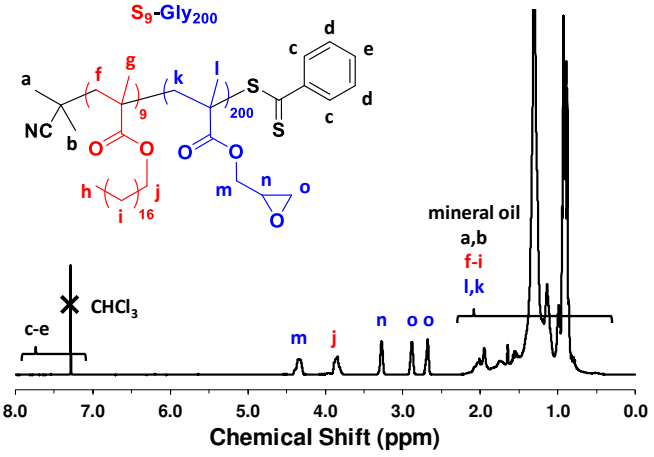

Figure 1. Assigned ^{1}H NMR spectrum recorded in $CDCl_3$ for a $PSMA_9$-$PGlyMA_{200}$ (S_9-Gly_{200}) diblock copolymer after its synthesis via RAFT dispersion polymerization in mineral oil at 70 °C and 30% w/w solids. The signals labelled n, o and o indicate epoxy group survival.

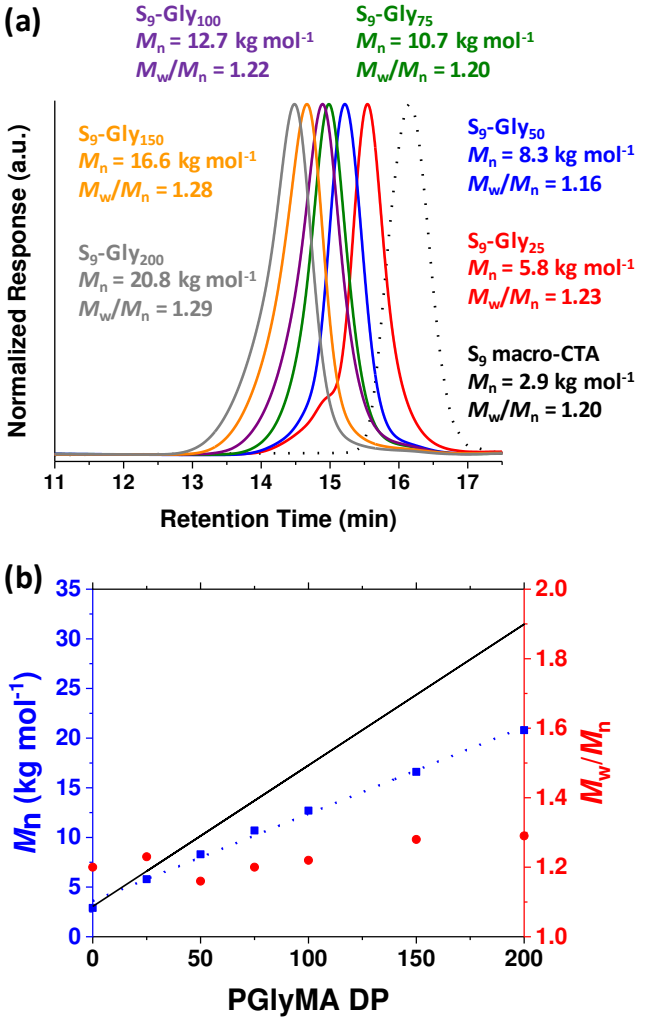

Figure 2. (a) Chloroform gel permeation chromatography curves (calibrated against a series of poly(methyl methacrylate) standards) obtained for a series of $PSMA_9$-PGlyMAx (denoted S_9-Gly_x) diblock copolymers prepared at 30% w/w solids via RAFT dispersion polymerization of GlyMA in mineral oil at 70 °C. Data for the $PSMA_9$ (S_9) precursor prepared in toluene at 70 °C and 50% w/w solids is also shown as a black dashed curve. (b) Variation in M_n (blue squares) and M_w/M_n (red circles) with target PGlyMA DP for the same series of S_9-Gly_x diblock copolymers (where x = 0 indicates the data obtained for the S_9 precursor). The black line indicates the theoretical M_n values while the blue dashed line is simply a guide to the eye, rather than a fit to the data. The deviation of the experimental M_n data from the theoretical values can be explained by the difference in hydrodynamic volume between the S_9-Gly_x diblock copolymer chains and the PMMA calibration standards.

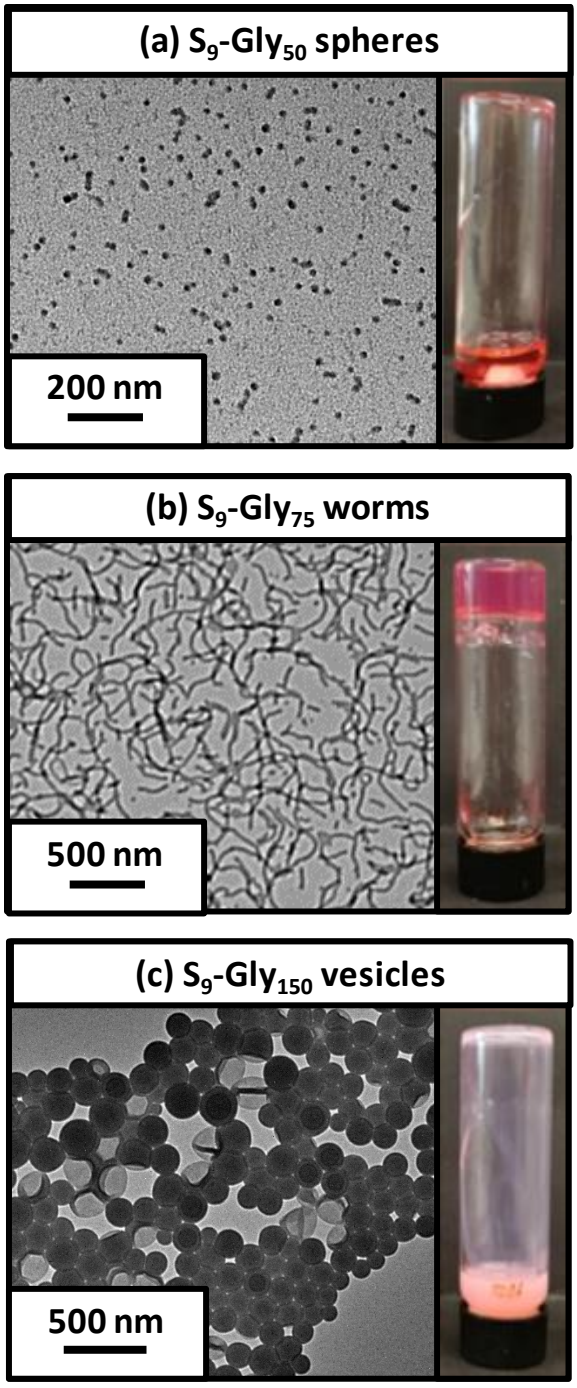

Figure 3. Representative transmission electron micrographs (obtained by drying 0.10% w/w dispersions) and inset digital photographs recorded for 30% w/w dispersions of (a) S_9-Gly_{50} spheres, (b) S_9-Gly_{75} worms and (c) S_9-Gly_{150} vesicles.

higher molecular weight compared to that of the $PSMA_9$ precursor (see Figure 2a).

Visual inspection of the copolymer dispersions can often provide an initial indication of the nanoparticle morphology.[51] Hence 30% w/w dispersions of S_9-Gly_{25} and S_9-Gly_{50} were both transparent and free-flowing, which is consistent with the presence of relatively small isotropic spheres. In contrast, dispersions of S_9-Gly_{75} and S_9-Gly_{100} formed relatively transparent free-standing gels. This indicates the presence of anisotropic worm-like particles, which form a 3D network via multiple inter-worm contacts.[52] Finally, S_9-Gly_{150} and S_9-Gly_{200} formed turbid, free-flowing dispersions, which suggests the presence of large (> 100 nm) isotropic particles such as spheres or vesicles. For more rigorous copolymer morphology assignments, TEM and DLS studies were performed. Small spherical nanoparticles were observed on TEM grids prepared using 0.10% w/w dispersions of S_9-Gly_{25} and S_9-Gly_{50} (see Figure

3a). DLS studies were consistent with these observations with intensity-average diameters of 27 nm and 31 nm being obtained, respectively. For S_9-Gly_{75} and S_9-Gly_{100}, DLS analysis indicated much larger diameters and relatively broad particle size distributions, which suggested the presence of worms and worm/vesicle clusters. Indeed, TEM studies confirmed that S_9-Gly_{75} formed a pure worm phase (see Figure 3b), whereas S_9-Gly_{100} produced a mixture of worms and vesicles (see Figure S1). DLS studies indicated intensity-average diameters of 170 nm and 190 nm and relatively narrow size distributions for S_9-Gly_{150} and S_9-Gly_{200}, respectively. TEM analysis of these two dispersions confirmed the formation of pure vesicles in both cases (e.g., see Figure 3c).

Although TEM studies usually enable copolymer morphologies to be assigned with reasonable confidence, this characterization technique can suffer from several artifacts. Firstly, TEM grid preparation involves staining to improve contrast. Moreover, only a relatively small number of nanoparticles can be assessed, so there is always the possibility that such limited sampling may not be truly representative of the copolymer morphology. One well-known limitation of DLS analysis is that the Stokes-Einstein equation assumes a spherical morphology, so the apparent intensity-average diameter determined for highly anisotropic nano-objects such as worms is neither representative of their mean length nor their mean cross-sectional radius.[28] In contrast, SAXS is a powerful analytical technique that does not suffer from such problems since it can provide the true particle dimensions by averaging over millions of nano-objects. In principle, SAXS can be conducted on concentrated copolymer dispersions in their 'wet' state, although relatively low concentrations (e.g. 1% w/w) are typically used in order to avoid inter-particle interactions. Moreover, there are well-established SAXS models for the analysis of spheres,[53] worms[53] and vesicles,[54] enabling rigorous characterization of these S_9-Gly_x dispersions regardless of their copolymer morphology. Accordingly, SAXS patterns were recorded for dilute dispersions of S_9-Gly_{50} spheres, S_9-Gly_{75} worms, and both S_9-Gly_{150} and S_9-Gly_{200} vesicles in mineral oil (see Figure 4) and subsequently fitted using the appropriate model in each case (see Supporting Information). Fitting the SAXS pattern obtained for S_9-Gly_{50} spheres required the use of a mixed spheres, dimers and trimers model.[55] Indeed, close inspection of the TEM image in Figure 3a reveals a minor population of partially fused spheres. The relative volume fractions of individual spheres ($\varphi_{spheres}$), dimers (φ_{dimers}) and trimers ($\varphi_{trimers}$) were 0.62, 0.29 and 0.09, respectively, while the mean diameter of the former species (D_{sphere}) was determined to be 17.0 ± 1.3 nm. This volume-average diameter is significantly smaller than the intensity-average diameter determined by DLS. This is because the latter technique cannot distinguish between single spheres, dimers and trimers, as suggested by the relatively high polydispersity index of 0.21. Accounting for the coexistence of spheres, dimers and trimers, the mean number of copolymer chains per nanoparticle (or aggregation number, N_{agg}) was estimated to be 321. The SAXS pattern recorded for S_9-Gly_{75} worms was fitted to a well-known worm-like micelle model,[53] which indicated a mean worm

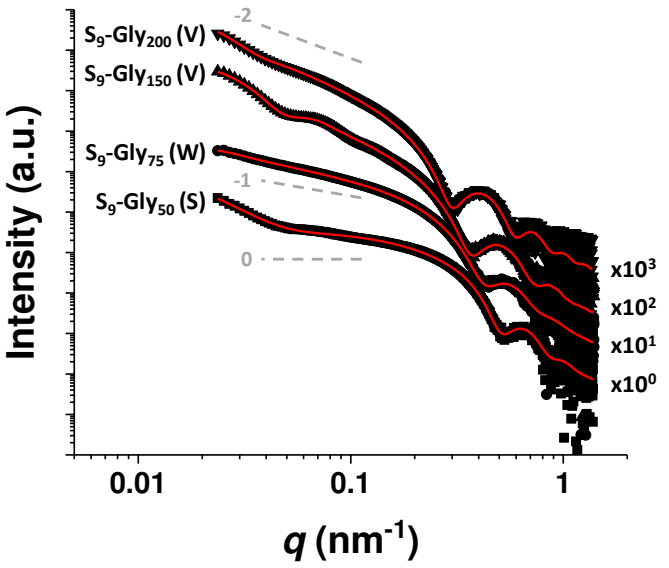

Figure 4. Small-angle X-ray scattering (SAXS) patterns recorded for 1.0% w/w dispersions of S_9-Gly_x diblock copolymer nano-objects in mineral oil at 25 °C (S, W and V denote spheres, worms and vesicles, respectively). Gradients of 0, -1 and -2 are provided as a guide to the eye. Data fits obtained using appropriate scattering models for a mixture of spheres, dimers and trimers,[55] worms[53] or vesicles[54] are represented by solid red lines.

thickness (T_{worm}) of 18.0 ± 1.6 nm, a mean worm length (L_{worm}) of 262 nm and an N_{agg} of 4085. Comparison of the N_{agg} values calculated for spheres and worms suggests that at least 13 spheres fuse together to produce each worm during the PISA synthesis of S_9-Gly_{75} worms. SAXS patterns recorded for both S_9-Gly_{150} and S_9-Gly_{200} nanoparticles could be satisfactorily fitted to a vesicle model.[54] For S_9-Gly_{150} vesicles, the volume- average vesicle diameter ($D_{vesicle}$) was determined to be 137 ± 21 nm, the vesicle membrane thickness ($T_{membrane}$) was 16.1 ± 1.8 nm and N_{agg} was around 25,500. The latter value suggests that, on average, approximately six worms combine to form each vesicle during the PISA synthesis of S_9-Gly_{150}. For S_9-Gly_{200} vesicles, $D_{vesicle}$ = 156 ± 37 nm, T_m = 19.6 ± 1.8 nm and N_{agg} = 30,200. A summary of all the key fitting parameters and nanoparticle dimensions obtained from SAXS data fits is provided in Table S1.

Oscillatory rheology measurements were conducted on a 30% w/w dispersion of S_9-Gly_{75} worms, which formed a free-standing gel at room temperature (see Figure 3b, inset digital image). An angular frequency sweep from 0.1 rad s^{-1} to 100 rad s^{-1} (conducted at 1.0% strain amplitude and 25 °C) confirmed that this dispersion behaved as a viscoelastic solid: the storage modulus (G') exceeded the loss modulus (G'') at all angular frequencies (see Figure S2a). Additionally, G' was relatively independent of angular frequency over this range, which corresponds to the linear viscoelastic region. A strain amplitude sweep from 0.1% to 100% (conducted at 10 rad s^{-1} and 25 °C) indicated linear viscoelastic behavior up to a critical strain amplitude of ~25-30% (see Figure S2b). A temperature sweep from 25 °C to 100 °C was performed within the linear viscoelastic region (strain amplitude = 1.0%, angular frequency = 10 rad s^{-1}) at a heating rate of 2 °C min^{-1} (see Figure 5a). At 25 °C, we find that G' = 7500 Pa and G'' = 1200 Pa. G' always

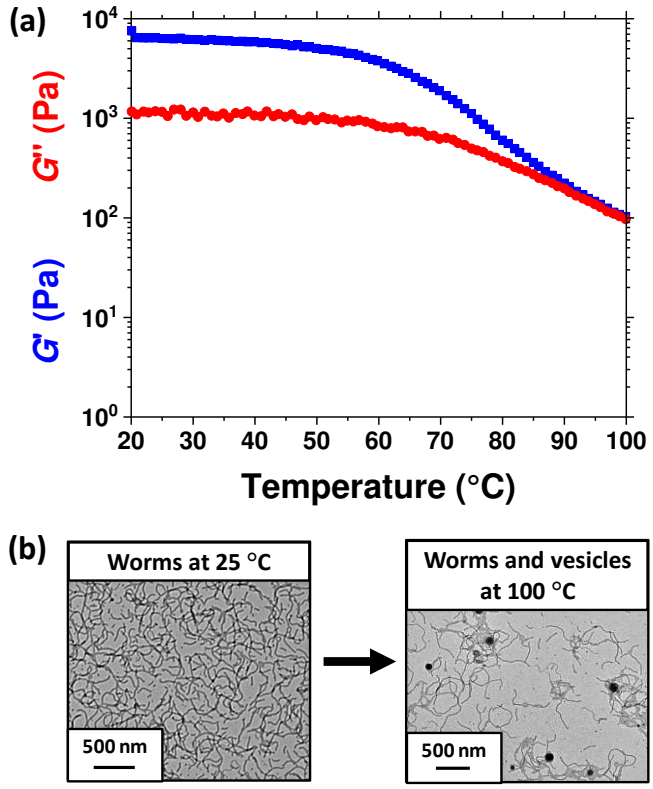

Figure 5. (a) Temperature dependence of the storage modulus (*G*', blue squares) and loss modulus (*G*", red circles) for a 30% w/w dispersion of $PSMA_9$-$PGlyMA_{75}$ worms in mineral oil on heating from 20 °C to 100 °C at 2 °C min^{-1}. Data were recorded every 30 s at 1.0% strain amplitude using an angular frequency of 10 rad s^{-1}. (b) TEM images show the predominant copolymer morphologies observed when diluting a 30% w/w dispersion to 0.10% w/w solids at 25 °C (left, pure worms) and 100 °C (right, worm/vesicle mixture).

remained significantly larger than *G*" on heating up to 60 °C, with higher temperatures leading to a significant reduction in both parameters. At 100 °C, *G*' = 102 Pa and *G*" = 97 Pa, which indicates that the gel changes from elastic, solid-like behavior (*G*' > *G*") to viscous, liquid-like behavior (*G*" > *G*') at this temperature. No critical gelation temperature (for which *G*' = *G*") could be identified in these experiments, although the copolymer dispersion became free-flowing at 100 °C. We and others have previously reported that PISA can be used to prepare thermoresponsive worm gels in various non-polar solvents.[24, 26, 28, 35, 56] These worms are transformed into spheres on heating owing to surface plasticization of the core-forming block by the ingress of hot solvent, which results in macroscopic degelation to produce a hot free-flowing fluid. TEM studies were performed to examine whether the gel softening observed for the present formulation was associated with a similar change in morphology. Accordingly, a small quantity (~ 0.2 g) of a 30% w/w dispersion of S_9-Gly_{75} worms was equilibrated at 100 °C for 1 h before being diluted to 0.10% w/w using *n*-dodecane which had been equilibrated *at the same temperature* in order to kinetically trap the block copolymer nano-objects present in the hot dispersion. This TEM preparation protocol revealed that the dispersion of pure S_9-Gly_{75} worms at 25 °C was converted into a mixture of worms and vesicles when heated up to 100 °C (see Figure 5b). This partial morphological transformation accounts for the gel softening that is observed on heating: as the volume fraction of worms is reduced, these highly anisotropic nanoparticles are no longer capable of forming a percolating gel network.[52] Moreover, the presence of a significant worm volume fraction at 100 °C accounts for the relatively high *G*' and *G*" values observed at this temperature, as well as the absence of a CGT. It is perhaps worth emphasizing that worm-to-vesicle transformations are known to be relatively slow and/or incomplete for several PISA formulations.[56, 57] Such a worm-to-vesicle transition must be facilitated by an increase in the volume of the insoluble structure-directing block relative to that of the soluble steric stabilizer block. This suggests that *surface* plasticization, which involves an effective increase in volume fraction for the latter block, does not occur in this case. We hypothesize that this partial worm-to-vesicle transition instead involves *uniform* solvation of the PGlyMA block, thus increasing its volume fraction. However, it remains unclear why PSMA-PGlyMA worms apparently undergo *uniform* solvation on heating, whereas closely-related worms comprising alternative structure-directing blocks exhibit *surface* plasticization.[21, 24, 28, 35, 39, 56] Such unexpected qualitative differences clearly warrant further investigation. Finally, it is noteworthy that this partial worm-to-vesicle transformation was not fully reversible on the time scale of the experiment, because some vesicles (and worm branch points) were still present after cooling to 25 °C (see Figure S3).

Conclusions

In summary, simply using a sufficiently short $PSMA_9$ steric stabilizer block for the RAFT dispersion polymerization of GlyMA in mineral oil enabled the formation of $PSMA_9$-$PGlyMA_x$ diblock copolymer spheres, worms or vesicles at 30% w/w solids as confirmed by DLS, TEM and SAXS analyses. THF GPC analysis indicated that reasonably good RAFT control (M_w/M_n < 1.30) was achieved for all PISA syntheses. A 30% w/w dispersion of $PSMA_9$-$PGlyMA_{75}$ worms formed a viscoelastic gel at 25 °C but underwent thermally-induced degelation when heated up to 100 °C; TEM studies indicated that a (partial) worm-to-vesicle morphological transformation under such conditions.

Conflicts of interest

There are no conflicts to declare.

Acknowledgements

S.P.A. acknowledges an EPSRC Established Career Fellowship (EP/R003009/1). The Leverhulme Trust is also thanked for post-doctoral support of M.J.D. (RPG-2016-330). The Lubrizol Corporation (Hazelwood, UK) is thanked for supplying the mineral oil used in this work.

References

1. B. Charleux, G. Delaittre, J. Rieger and F. D'Agosto, *Macromolecules*, 2012, **45**, 6753-6765.
2. N. J. Warren and S. P. Armes, *Journal of the American Chemical Society*, 2014, **136**, 10174-10185.
3. J. Tan, H. Sun, M. Yu, B. S. Sumerlin and L. Zhang, *ACS Macro Letters*, 2015, **4**, 1249-1253.
4. M. J. Derry, L. A. Fielding and S. P. Armes, *Progress in Polymer Science*, 2016, **52**, 1-18.
5. S. L. Canning, G. N. Smith and S. P. Armes, *Macromolecules*, 2016, **49**, 1985-2001.
6. N. J. W. Penfold, J. Yeow, C. Boyer and S. P. Armes, *ACS Macro Letters*, 2019, **8**, 1029-1054.
7. F. D'Agosto, J. Rieger and M. Lansalot, *Angewandte Chemie International Edition*, 2019, 10.1002/ange.201911758.
8. J. Chiefari, R. T. A. Mayadunne, C. L. Moad, G. Moad, E. Rizzardo, A. Postma, M. A. Skidmore and S. H. Thang, *Macromolecules*, 2003, **36**, 2273-2283.
9. G. Moad, E. Rizzardo and S. H. Thang, *Accounts of Chemical Research*, 2008, **41**, 1133-1142.
10. S. Perrier, *Macromolecules*, 2017, **50**, 7433-7447.
11. J. Rieger, F. Stoffelbach, C. Bui, D. Alaimo, C. Jerome and B. Charleux, *Macromolecules*, 2008, **41**, 4065-4068.
12. J. Rieger, C. Grazon, B. Charleux, D. Alaimo and C. Jérôme, *Journal of Polymer Science Part A: Polymer Chemistry*, 2009, **47**, 2373-2390.
13. Y. Li and S. P. Armes, *Angewandte Chemie-International Edition*, 2010, **49**, 4042-4046.
14. C. Grazon, J. Rieger, N. Sanson and B. Charleux, *Soft Matter*, 2011, **7**, 3482-3490.
15. I. Chaduc, W. J. Zhang, J. Rieger, M. Lansalot, F. D'Agosto and B. Charleux, *Macromolecular Rapid Communications*, 2011, **32**, 1270-1276.
16. C. A. Figg, A. Simula, K. A. Gebre, B. S. Tucker, D. M. Haddleton and B. S. Sumerlin, *Chemical Science*, 2015, **6**, 1230-1236.
17. Q. Qu, G. Liu, X. Lv, B. Zhang and Z. An, *ACS Macro Letters*, 2016, **5**, 316-320.
18. W.-M. Wan, X.-L. Sun and C.-Y. Pan, *Macromolecular Rapid Communications*, 2010, **31**, 399-404.
19. W. Zhao, G. Gody, S. M. Dong, P. B. Zetterlund and S. Perrier, *Polymer Chemistry*, 2014, **5**, 6990-7003.
20. Y. Pei and A. B. Lowe, *Polymer Chemistry*, 2014, **5**, 2342-2351.
21. Y. W. Pei, N. C. Dharsana, J. A. Van Hensbergen, R. P. Burford, P. J. Roth and A. B. Lowe, *Soft Matter*, 2014, **10**, 5787-5796.
22. Y. Pei, N. C. Dharsana and A. B. Lowe, *Australian Journal of Chemistry*, 2015, **68**, 939-945.
23. W.-J. Zhang, C.-Y. Hong and C.-Y. Pan, *Macromolecular Rapid Communications*, 2015, **36**, 1428-1436.
24. L. A. Fielding, M. J. Derry, V. Ladmiral, J. Rosselgong, A. M. Rodrigues, L. P. D. Ratcliffe, S. Sugihara and S. P. Armes, *Chemical Science*, 2013, **4**, 2081-2087.
25. A. P. Lopez-Oliva, N. J. Warren, A. Rajkumar, O. O. Mykhaylyk, M. J. Derry, K. E. B. Doncom, M. J. Rymaruk and S. P. Armes, *Macromolecules*, 2015, **48**, 3547-3555.
26. Y. Pei, O. R. Sugita, L. Thurairajah and A. B. Lowe, *RSC Advances*, 2015, **5**, 17636-17646.
27. Y. Pei, J.-M. Noy, P. J. Roth and A. B. Lowe, *Journal of Polymer Science Part A: Polymer Chemistry*, 2015, **53**, 2326-2335.
28. L. A. Fielding, J. A. Lane, M. J. Derry, O. O. Mykhaylyk and S. P. Armes, *Journal of the American Chemical Society*, 2014, **136**, 5790-5798.
29. L. Houillot, C. Bui, M. Save, B. Charleux, C. Farcet, C. Moire, J.-A. Raust and I. Rodriguez, *Macromolecules*, 2007, **40**, 6500-6509.
30. L. Houillot, C. Bui, C. Farcet, C. Moire, J.-A. Raust, H. Pasch, M. Save and B. Charleux, *ACS Applied Materials & Interfaces*, 2010, **2**, 434-442.
31. Y. Pei, L. Thurairajah, O. R. Sugita and A. B. Lowe, *Macromolecules*, 2015, **48**, 236-244.
32. E. J. Cornel, S. van Meurs, T. Smith, P. S. O'Hora and S. P. Armes, *Journal of the American Chemical Society*, 2018, **140**, 12980-12988.
33. M. J. Derry, L. A. Fielding and S. P. Armes, *Polymer Chemistry*, 2015, **6**, 3054-3062.
34. M. J. Derry, L. A. Fielding, N. J. Warren, C. J. Mable, A. J. Smith, O. O. Mykhaylyk and S. P. Armes, *Chemical Science*, 2016, **7**, 5078-5090.
35. M. J. Derry, O. O. Mykhaylyk and S. P. Armes, *Angewandte Chemie International Edition*, 2017, **56**, 1746-1750.
36. M. J. Derry, T. Smith, P. S. O'Hora and S. P. Armes, *ACS Applied Materials & Interfaces*, 2019.
37. P. J. Docherty, M. J. Derry and S. P. Armes, *Polymer Chemistry*, 2019, **10**, 603-611.
38. M. J. Rymaruk, S. J. Hunter, C. T. O'Brien, S. L. Brown, C. N. Williams and S. P. Armes, *Macromolecules*, 2019, **52**, 2882-2832.
39. M. J. Rymaruk, C. T. O'Brien, S. L. Brown, C. N. Williams and S. P. Armes, *Macromolecules*, 2019, **52**, 6849-6860.
40. K. L. Thompson, C. J. Mable, J. A. Lane, M. J. Derry, L. A. Fielding and S. P. Armes, *Langmuir*, 2015, **31**, 4137-4144.
41. K. L. Thompson, L. A. Fielding, O. O. Mykhaylyk, J. A. Lane, M. J. Derry and S. P. Armes, *Chemical Science*, 2015, **6**, 4207-4214.
42. P. Chambon, A. Blanazs, G. Battaglia and S. P. Armes, *Langmuir*, 2012, **28**, 1196-1205.
43. J. R. Lovett, L. P. D. Ratcliffe, N. J. Warren, S. P. Armes, M. J. Smallridge, R. B. Cracknell and B. R. Saunders, *Macromolecules*, 2016, **49**, 2928-2941.
44. F. L. Hatton, J. R. Lovett and S. P. Armes, *Polymer Chemistry*, 2017, **8**, 4856-4868.
45. J. Tan, D. Liu, C. Huang, X. Li, J. He, Q. Xu and L. Zhang, *Macromolecular Rapid Communications*, 2017, **38**, 1700195.
46. C. György, J. R. Lovett, N. J. W. Penfold and S. P. Armes, *Macromolecular Rapid Communications*, 2018, 1800289.
47. F. L. Hatton, A. M. Park, Y. Zhang, G. D. Fuchs, C. K. Ober and S. P. Armes, *Polymer Chemistry*, 2019, **10**, 194-200.
48. B. Couturaud, P. G. Georgiou, S. Varlas, J. R. Jones, M. C. Arno, J. C. Foster and R. K. O'Reilly, *Macromolecular Rapid Communications*, 2019, **40**, 1800460.
49. J. S. Trent, *Macromolecules*, 1984, **17**, 2930-2931.
50. J. Ilavsky and P. R. Jemian, *Journal of Applied Crystallography*, 2009, **42**, 347-353.
51. L. P. D. Ratcliffe, B. E. McKenzie, G. M. D. Le Bouëdec, C. N. Williams, S. L. Brown and S. P. Armes, *Macromolecules*, 2015, **48**, 8594-8607.

52. J. R. Lovett, M. J. Derry, P. Yang, F. L. Hatton, N. J. Warren, Patrick W. Fowler and S. P. Armes, *Chemical Science*, 2018, **9**, 7138-7144.
53. J. S. Pedersen, *Journal of Applied Crystallography*, 2000, **33**, 637-640.
54. J. Bang, S. M. Jain, Z. B. Li, T. P. Lodge, J. S. Pedersen, E. Kesselman and Y. Talmon, *Macromolecules*, 2006, **39**, 1199-1208.
55. N. J. Warren, O. O. Mykhaylyk, D. Mahmood, A. J. Ryan and S. P. Armes, *Journal of the American Chemical Society*, 2014, **136**, 1023-1033.
56. Y. Pei, A. B. Lowe and P. J. Roth, *Macromolecular Rapid Communications*, 2017, **38**, 1600528.
57. J. R. Lovett, N. J. Warren, L. P. D. Ratcliffe, M. K. Kocik and S. P. Armes, *Angewandte Chemie International Edition*, 2015, **54**, 1279-1283.

